J. Fluid Mech. (1986), *vol.* 169, *pp.* 1–26
Printed in Great Britain

Thermocapillary free boundaries in crystal growth

By C. CUVELIER AND J. M. DRIESSEN†
Delft University of Technology, Department of Mathematics and Informatics, Delft, The Netherlands

(Received 5 June 1985 and in revised form 29 October 1985)

In this paper a two-dimensional free boundary arising from the steady thermocapillary flow in a viscous incompressible fluid is studied numerically. The problem is considered in the context of the open-boat crystal-growth technique. The motion of the fluid is governed by the Navier–Stokes equations coupled with the heat equation. The problem is solved numerically by a finite-element-method discretization. Three iterative methods are introduced for the computation of the free boundary. The non-dimensional form of the problem gives rise to the following characteristic parameters: Reynolds, Grashof, Prandtl, Marangoni, Bond, Ohnesorge, Biot numbers. The influence of these parameters on the flow field, the temperature distribution and the shape of the free boundary is studied.

1. Introduction

Many problems in physics and mechanics can be described by partial differential equations for the unknown functions. When there are additional geometrical unknowns they are known as free-boundary problems. In general, one defines a free-boundary problem as a boundary-value problem involving (partial) differential equations on domains, parts of whose boundaries, the free boundaries, are unknown and must be determined as part of the solution.

In hydrodynamics classical unknowns are, for instance, the velocity vector and the pressure distribution in the fluid. Free boundaries can be present as a liquid–gas interface or the interface of two immiscible liquids. Capillary free boundaries are defined as free boundaries on which one must take into account capillary forces, i.e. forces due to intermolecular attractions having a non-vanishing resultant at the boundary of the liquid.

There are many important technological and engineering-science applications in which capillary free boundaries play a dominant part, for example in lubrication, electrochemical plating, corrosion, coating, polymer technology, separation processes, metal and glass forming processes, crystal growth and aerospace technology, there are abundant technologically important fluid flows with capillary free boundaries.

A situation of special interest, both from the technological and the purely mathematical point of view, is the study of the behaviour of liquids in an open container in a low-g environment, where capillary free boundaries must be taken into account. These problems have been studied in Greenspan (1968), Guibert, Huynh & Marce (1976) and Moiseev & Rumyantsev (1968) for inviscid fluids in relation to aerospace technology (attitude control of spacecraft and satellites). For a study of viscous capillary stationary free boundaries, we refer to Cuvelier (1982, 1985*a*),

† Present address: Koninklijke/Shell-Laboratorium, Amsterdam, Shell Research bv, Amsterdam, The Netherlands

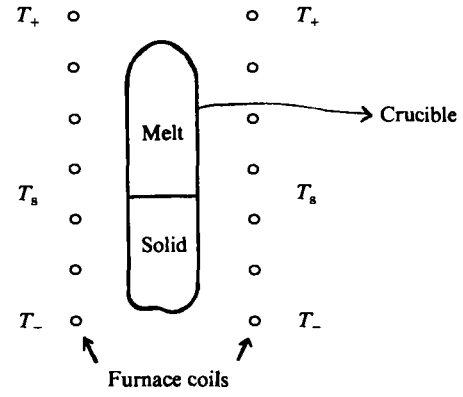

FIGURE 1. The Bridgman technique. The crucible is moved down a temperature gradient $T_+ > T_s > T_-$ with T_s the solidification temperature.

Pukhnachev (1974) and Solonnikov (1979). Non-stationary capillary free boundaries have been investigated in Allain (1984) and Beale (1984) and from a numerical point of view in Cuvelier (1985*b*).

In this paper we shall focus our attention on the (finite-element) analysis of thermocapillary free boundaries in crystal-growth processes. Crystal growth, by definition, is concerned with the formation of a single crystal, by which we mean a solid in the most uniform structure that can be attained. This uniform structure of crystals, which can be modified by the controlled addition of impurities, allows, for instance, the transmission without scattering of electromagnetic waves and charged particles and forms the basis of the electronic-industrial fabrication of devices like chips, transistors, semi-conductors, etc. When we survey the crystal-growth methods, we see that the technique where crystals grow from a melt is the most widely used one for the preparation of large single crystals. For a review of this type of method we refer to Brice (1965), Hartman (1973), Hurle & Jakeman (1981) and Pimputkar & Ostrach (1981). All growth-from-the-melt or solidification methods have in common that the melt is cooled below its freezing point, the melt solidifies and the solid (crystal)–melt interface is advancing into the melt region.

Melt growth techniques can be subdivided into three groups:

(i) Those of Bridgman, Stober and Kapitza, where the melt is contained in a crucible and is progressively solidified from one end by moving the crucible relative to a temperature gradient (see figure 1). One disadvantage of such techniques is that a part of the liquid (melt)–solid (crystal) interface is in contact with the crucible.

(ii) Those of Czochralski and Kyropoulos, and also variants of these (like for instance the Pedestal technique), are widely used. The melt is contained in a crucible and the crystal grows at the free melt surface in such a way that there is no contact between the crucible and the crystal. In the Czochralski process (see figure 2) the crystal is pulled slowly out of the melt. In the Kyropoulos variant the temperature of the melt is lowered, so that the crystal grows into the melt. The advantage of this group of techniques is that the liquid–solid interface is not in contact with the crucible.

(iii) In the third group the melt is supported by its own solid and crucibles are eliminated. A molten zone is maintained by surface tension in the rod of solid and is moved slowly with respect to furnace coils. Particular examples of these techniques are the floating-zone technique (see figure 3), where the rod is in the direction of

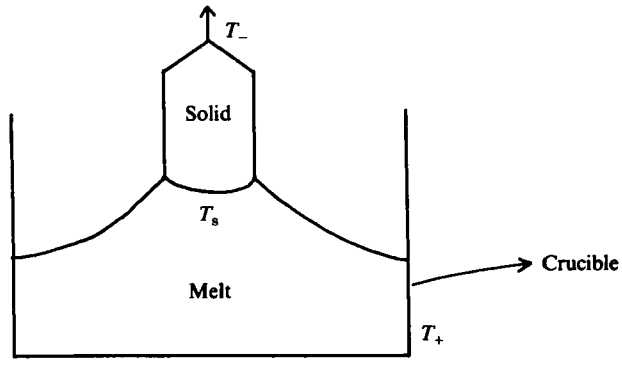

FIGURE 2. The Czochralski technique. The crystal is pulled out of the melt. $T_+ > T_s > T_-$, T_s is the solidification temperature.

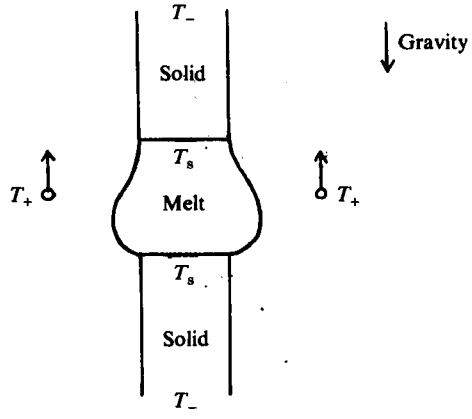

FIGURE 3. The floating-zone technique. The furnace coils are slowly moved upward. $T_+ > T_s > T_-$, T_s solidification/melting temperature.

gravity, and the open-boat-zone technique, where the rod is directed perpendicular to gravity. A disadvantage of this technique is that a high surface tension is required. On the other hand it can be repeated many times, which can be an important feature when the crystal must be doped with impurities. Moreover, only a part of the charge is molten at any time.

As we can see from these three growth techniques, there are, in general, two types of free boundaries. The first is the crystal–melt interface. The determination of this interface is reminiscent of the so-called Stefan problem, because heat transfer in the crystal and in the melt is coupled by requirements of temperature continuity and energy conservation. In the heat-flux balance on this interface, the latent heat must be taken into account since it determines the growth rate of the crystal into the melt.

The second kind of free boundary is the liquid–air interface. According to the basic principles of hydrodynamics the condition of a balance of forces must be fulfilled on this free boundary. Surface tension and the temperature dependence of the surface-tension coefficient must be taken into account, since they influence the flow pattern of the melt and consequently the temperature distribution near the crystal. This temperature distribution near the crystal in turn affects the crystal morphology and growth rate.

The possibility nowadays of using the space shuttles to carry a manned space laboratory has intensified interest in the concept of crystal manufacturing in space. Prolonged periods in a microgravity environment of about $10^{-3}\,g$–$10^{-6}\,g$ can be achieved in a near-Earth orbit, where g denotes the terrestrial gravity. The importance of a low-g environment for crystal growth is that natural convection (i.e. convection due to density variations in the melt) can be reduced considerably. Moreover, it was found that in a low-g situation more homogeneous and less striated crystals can be produced. Although it is not certain whether there are crystals for use in commercial electronic devices which can only be manufactured in space and whose quality is unattainable on Earth, crystal-growth experiments or, in general, the behaviour of liquids in space can help us to understand fundamental physical processes, in particular when these experiments are complemented by terrestrial experiments, mathematical modelling and numerical analysis (for reviews see Curruthers 1977; Cuvelier 1982; Haynes 1979; Ostrach 1976, 1982; and Pimputkar & Ostrach 1981). Although, as mentioned above, a low-g environment can reduce substantially the phenomenon of natural convection due to density variation in the melt, other types of convection processes become important. The presence of a free melt–gas interface can influence the motion of the melt when the coefficient of surface tension varies from point to point. In a non-isothermal melt there will be a surface-tension gradient on the melt–gas interface because of the temperature dependence of the surface-tension coefficient. This surface-tension gradient acts like a shear stress on the melt–gas interface and thereby generates a surface flow from the region of low surface tension to that of high surface tension, which usually means from hot to cold. Owing to the viscosity of the melt this surface motion penetrates into the melt and induces a bulk flow. This type of convection is called Marangoni or thermocapillary convection. For reviews on surface-tension phenomena we refer to Ostrach (1977, 1979, 1982), Schwabe (1981) and Schwabe & Scharmann (1981).

The aim of this paper is to investigate stationary (melt–gas) free-boundary problems in the context of crystal growth from the numerical point of view. As we have mentioned above, the crystal growth system is subjected to two types of convection. The first is the convection due to gravitational buoyancy forces (which we call Grashof convection). The second is induced by a gradient of the surface-tension coefficient (called Marangoni convection).

We shall study the relative influence of these two types of convection on the shape of the melt–gas free boundary. The melt–crystal interface shape is not considered in this paper and is assumed to be constant. Since one needs to solve the general hydrodynamic equations based on the Navier–Stokes equations, it is evident that the analytical or numerical study of this type of free-boundary problem is difficult. This is why we shall restrict ourselves to a model problem of open-boat type which has some relevance from the crystal growth point of view and which is general enough to admit a realistic study of free-boundary shapes. Although some limitations exist when comparing with real crystal-growth techniques, the open-boat situation to be discussed in this paper can serve as a model for various crystal-growth configurations.

In §2 we formulate the open-boat-model problem and write the (partial differential) equations governing the melt flow field. The equations are written in dimensionless form and characteristic numbers (Reynolds, Grashof, Prandtl, Marangoni, Biot, Bond, Ohnesorge) are introduced. In §3 we treat some iterative methods for the computation of the free-boundary shape and make some remarks concerning the finite-element discretization of the system. Finally, in §4 we present and discuss the results of numerical experiments.

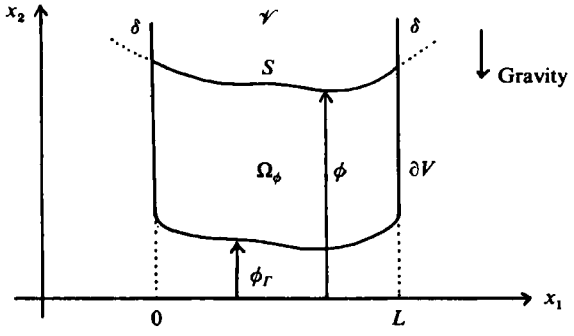

FIGURE 4. Liquid contained in a vessel $\mathscr{V}$.

2. The mathematical model

The problem we shall consider is the stationary motion of a liquid in an open vessel $\mathscr{V}$ placed in the field of gravity $\begin{pmatrix} 0 \\ -g \end{pmatrix}$. We suppose that $\mathscr{V}$ is given by

$$\mathscr{V} = \{\boldsymbol{x} = \{x_1, x_2\} \in \mathbb{R}^2 \mid x_2 > \phi_\Gamma(x_1), \quad 0 < x_1 < L\}, \tag{2.1}$$

where $\phi_\Gamma : x_1 \to \phi_\Gamma(x_1)$ is such that the container wall $\partial\mathscr{V}$ is sufficiently smooth (see figure 4).

When the fluid is in stationary motion the position of the fluid surface S, which is represented by a function $\phi : x_1 \in (0, L) \to \phi(x_1)$ (see figure 4) is not known *a priori* and is called a free boundary. The object is to find the shape of this free boundary. The equations describing the dynamics of the fluid flow can be derived from the basic principles of conservation of mass, momentum and energy.

These basic equations can be simplified by making the following assumptions (cf. Batchelor 1967; Landau & Lifchitz 1963). We assume that the Boussinesq approximation is valid, which means that variations in the density ρ_0 are negligible, except in the body-force term of the equation of conservation of momentum, where the variations induced by temperature gradients give rise to a body force $-\begin{pmatrix} 0 \\ g\rho \end{pmatrix}$, where ρ satisfies the following relation of state:

$$\rho = \rho_0(1 - \beta(T - T_0)), \tag{2.2}$$

where T denotes the temperature, $\beta \equiv -1/\rho_0 \, (\mathrm{d}\rho/\mathrm{d}T)|_{T_0}$ is the volume expansion coefficient and where the subscript 0 refers to a reference state. We neglect the mechanical-energy term in the equation of conservation of energy and we assume that the viscosity μ, the thermal conductivity k and the specific heat c_p at constant pressure are constant.

With these assumptions the stationary equations of conservation of momentum, mass and energy reduce to the well-known Navier–Stokes equations coupled with the heat-conduction equation for the velocity $\boldsymbol{u} = \{u_1, u_2\}$, the pressure p and the temperature T

$$-\mu \, \Delta \boldsymbol{u} + \rho_0(\boldsymbol{u} \cdot \nabla)\boldsymbol{u} + \nabla p = \rho_0 g(1 - \beta(T - T_0)) \begin{pmatrix} 0 \\ -1 \end{pmatrix}, \tag{2.3}$$

$$\nabla \cdot \boldsymbol{u} = 0, \tag{2.4}$$

$$-k \, \Delta T + c_p \rho_0 (\boldsymbol{u} \cdot \nabla) T = 0, \tag{2.5}$$

in the region Ω_ϕ defined by

$$\Omega_\phi = \{x = \{x_1, x_2\} \in \mathscr{V} \mid x_2 < \phi(x_1)\}. \tag{2.6}$$

In the equation we have ∇ the gradient operator and the Laplace operator Δ. A body force per unit mass f or a heat-source density q can be added to the right-hand side of (2.3) or (2.5) respectively. The boundary conditions are as follows: on $\Gamma = \partial V \cap \partial\Omega_\phi$ we describe Dirichlet boundary conditions for the velocity

$$u = \tilde{h}_u \quad \text{on } \Gamma \tag{2.7}$$

According to the basic principles of hydrodynamics, the conditions of a balance of forces must be fulfilled on the free boundary. These conditions are the so-called traction conditions on S for the normal stress σ_ν and the tangential stress σ_τ:

$$\sigma_\nu \equiv \sigma_\nu(p, u) \equiv \sum_{i,j=1}^{2} \sigma_{ij} \nu_i \nu_j \equiv -p + 2\mu \frac{\partial u}{\partial \nu} \cdot \nu = \frac{\gamma}{R} - p_a \quad \text{on } S, \tag{2.8}$$

$$\sigma_\tau \equiv \sigma_\tau(u) \equiv \sum_{i,j=1}^{2} \sigma_{ij} \nu_i \tau_j \equiv \frac{\partial u}{\partial \nu} \cdot \tau + \frac{\partial u}{\partial \tau} \cdot \nu = \frac{\partial \gamma}{\partial \tau} \quad \text{on } S, \tag{2.9}$$

where

$$\sigma_{ij} = -p\delta_{ij} + \mu\left(\frac{\partial u_i}{\partial x_j} + \frac{\partial u_j}{\partial x_i}\right) \tag{2.10}$$

and where $\nu = \{\nu_1, \nu_2\}$ denotes the unit outward normal on S, $\tau = \{\tau_1, \tau_2\} = \{\nu_2, -\nu_1\}$ the unit tangent on S, γ the surface-tension coefficient and p_a the outside (atmospheric) pressure which we put equal to zero. R denotes the radius of curvature of S, defined by

$$\frac{1}{R} = \left\{\frac{\phi'}{\{1 + |\phi'|^2\}^{\frac{1}{2}}}\right\}', \quad \text{where } ' = \frac{\mathrm{d}}{\mathrm{d}x_1}. \tag{2.11}$$

Surface tension is a thermodynamic property depending on temperature. Variations in temperature cause shear stress which can influence by an order of magnitude the rates of transport of momentum and heat near the free surface. This type of phenomenon is called the Marangoni (or thermocapillary) effect. The surface-tension coefficient of a pure liquid in equilibrium with its own vapour or with a gas decreases almost linearly with temperature until a critical temperature is approached. For the modest velocities and temperature differences that we assume, the surface-tension coefficient can be considered as a linear function of temperature:

$$\gamma = \gamma_0(1 - \alpha(T - T_0)), \tag{2.12}$$

where $\alpha = -(1/\gamma_0)\,(\mathrm{d}\gamma/\mathrm{d}T)\,|_{T_0}$ is the temperature coefficient of surface tension and where the subscript 0 refers to a reference state. In general, the value of α is positive and for many crystals, e.g. Si, $NaNO_3$, Al_2O_3, ... its value is less than 5×10^{-4}. Relation (2.12) is known as the Eötvos formula and is applicable for a large number of liquids (cf. Barbe 1967; Hardy 1985).

We now make the following Boussinesq-type approximation with respect to the surface tension. We assume that the surface-tension coefficient γ equals a constant γ_0 independent of temperature, except in the boundary condition (2.9) where γ depends on temperature according to (2.12). The stress boundary conditions (2.8), (2.9) on the free boundary S now take the following form:

$$\sigma_\nu = \frac{\gamma_0}{R} \quad \text{on } S, \tag{2.13}$$

$$\sigma_\tau = -\alpha\gamma_0 \frac{\partial T}{\partial \tau} \quad \text{on } S. \tag{2.14}$$

This approximation is widely applicable and is justified by an order-of-magnitude analysis. In practical situations the variation in temperature along the free surface never exceeds 100 °C, so that the relative change in the normal stress due to temperature is less than approximately $5\times10^{-4}\times\frac{100}{2}=0.025$.

For a stationary fluid motion, the free boundary is a streamline which implies the following kinematic condition:

$$u_\nu \equiv \boldsymbol{u}\cdot\boldsymbol{\nu}=0 \quad \text{on } S. \tag{2.15}$$

Moreover the free boundary must satisfy the condition that the contact angle δ between S and the container wall (measured within the fluid) is prescribed (see figure 4):

$$\phi'(0)=-\operatorname{cotan}\delta, \quad \phi'(1)=\operatorname{cotan}\delta. \tag{2.16}$$

Concerning the boundary conditions for the temperature, we assume that the temperature is given on the container wall:

$$T=\tilde{h}_T \quad \text{on } \Gamma, \tag{2.17}$$

and that the following radiation condition holds on the free boundary in combination with Newton's law of cooling:

$$-k\frac{\partial T}{\partial \nu}=\epsilon\sigma(T^4-T_{\text{inf}}^4)+\eta(T-T_{\text{amb}})^{1.25} \quad \text{on } S \tag{2.18}$$

where ϵ is the emissivity, σ the Stefan–Boltzmann constant, T_{inf} the temperature of the bounding gas far from the interface, η the heat-transfer coefficient and T_{amb} the ambient gas temperature.

Finally we specify the quantity of fluid $\tilde{V}_c$ in the vessel $\mathscr{V}$ by

$$\int_{\Omega_\phi} \mathrm{d}x = \tilde{V}_c \text{ given}. \tag{2.19}$$

The relation of this model to real crystal-growth situations is as follows (cf. Schwabe & Scharmann 1981). Open-boat zoning is simulated if the boundary Γ has constant temperature T_s and when the free boundary S is heated by a furnace coil of temperature $T_+ > T_s$. The vertical sides of the vessel can then be interpreted as the melt–crystal interface, the bottom of the vessel represents the boat (crucible) and S is the melt–gas interface. The Czochralski technique is simulated when the left-hand vertical side of $\mathscr{V}$ (the crucible) is at temperature T_+ and the right-hand vertical side of $\mathscr{V}$ (the crystal) at temperature $T_s < T_+$.

The equations will now be written in dimensionless form. We introduce a lengthscale L, a velocity scale U which will be specified later and we obtain the following dimensionless quantities:

$$\hat{x}=\frac{x}{L}, \quad \hat{\boldsymbol{u}}=\frac{\boldsymbol{u}}{U}, \quad \hat{p}=\frac{1}{\rho U^2}(p+\rho_0 g x_2), \quad \hat{T}=\frac{T}{\delta T},$$

where $\delta T = T_+ - T_s$ with $T_+ = \max(\tilde{h}_T)$, $T_s = \min(\tilde{h}_T)$. When we take $T_0 = \frac{1}{2}(T_+ + T_s)$, the problem in dimensionless form is formulated as follows (where we have dropped the $\hat{}$):

Find a free boundary ϕ, a velocity vector $\boldsymbol{u}=\{u_1, u_2\}$, a pressure field p and a temperature field T such that

$$\left.\begin{aligned} -\frac{1}{Re}\Delta\boldsymbol{u}+(\boldsymbol{u}\cdot\nabla)\boldsymbol{u}+\nabla p &= \frac{Gr}{Re^2}(T-T_0)\begin{pmatrix}0\\1\end{pmatrix}, && (2.20)\\ \nabla\cdot\boldsymbol{u}&=0, && (2.21)\\ -\frac{1}{Re\,Pr}\Delta T+(\boldsymbol{u}\cdot\nabla)T&=0, && (2.22)\end{aligned}\right\} \text{ in } \Omega_\phi$$

$$\left.\begin{aligned} \boldsymbol{u} &= \frac{\boldsymbol{h}_u}{Re}, \\ T &= h_T, \end{aligned}\right\} \quad \text{on } \Gamma \tag{2.23}$$

$$(Oh\ Re)^2 \sigma_\nu = \frac{1}{R} - Bo\,\phi, \tag{2.25}$$

$$\sigma_\tau = -\frac{Ma}{Re^2\,Pr}\frac{\partial T}{\partial \tau}, \tag{2.26}$$

$$u_\nu = 0, \tag{2.27}$$

$$-\frac{1}{Re\,Pr}\frac{\partial T}{\partial \nu} = \frac{Bi_r}{Re\,Pr}(T^4 - T_{inf}^4) + \frac{Bi_c}{Re\,Pr}(T - T_{amb})^{1.25}, \tag{2.28}$$

$$\text{on } S$$

$$\phi'(0) = -\operatorname{cotan}\delta, \quad \phi'(1) = \operatorname{cotan}\delta, \tag{2.29}$$

$$\int_{\Omega_\phi} \mathrm{d}x = V_c, \tag{2.30}$$

where

$$\Omega_\phi = \{\boldsymbol{x} \in \mathscr{V} \mid x_2 < \phi(x_1)\}, \quad \mathscr{V} = \{\boldsymbol{x} = \{x_1, x_2\} \mid 0 < x_1 < 1,\ x_2 > \phi_\Gamma(x_1)\},$$

$$Re = \frac{LU\rho_0}{\mu} \quad \text{Reynolds number},$$

$$Gr = \frac{\beta g \rho_0^2 L^3 \delta T}{\mu^2} \quad \text{Grashof number},$$

$$Pr = \frac{c_p \mu}{k} \quad \text{Prandtl number},$$

$$Oh = \frac{\mu}{(\rho_0 \gamma_0 L)^{\frac{1}{2}}} \quad \text{Ohnesorge number},$$

$$Bo = \frac{g\rho_0 L^2}{\gamma_0} \quad \text{Bond number},$$

$$Ma = \frac{\alpha \gamma_0 c_p \rho_0 L \delta T}{\mu k} \quad \text{Marangoni number},$$

$$\boldsymbol{h}_u = \frac{\tilde{\boldsymbol{h}}_u L \rho_0}{\mu}, \quad h_T = \frac{\tilde{h}_T}{\delta T},$$

$$Bi_r = \frac{\epsilon \sigma L (\delta T)^3}{k} \quad \text{Biot number for radiation},$$

$$Bi_c = \frac{\eta L (\delta T)^{1.25}}{k} \quad \text{Biot number for cooling},$$

$$\sigma_{ij} = -p\delta_{ij} + \frac{1}{Re}\left(\frac{\partial u_i}{\partial x_j} + \frac{\partial u_j}{\partial x_i}\right),$$

$$V_c = \frac{\tilde{V}_c}{L^2}.$$

Concerning the choice of the characteristic velocity U, when $\tilde{\boldsymbol{h}}_u \not\equiv 0$ it is obvious to take $U = \max|\tilde{\boldsymbol{h}}_u|$. When $\tilde{\boldsymbol{h}}_u \equiv 0$, we can take $U = \mu/L\rho_0$ which is equivalent to taking $Re = 1$ in the system of equations.

From the equations it is evident that a necessary condition for a static equilibrium (i.e. no fluid motion, $\boldsymbol{u} \equiv 0$) to exist is that the Marangoni number is equal to zero (unless the fluid is isothermal). In the static equilibrium with $Ma = Gr = 0$, the pressure p_* and the free boundary ϕ_* are completely determined by (2.20), (2.25), (2.29), (2.30). One easily verifies that, for V_c sufficiently large, ϕ_* is determined by the following boundary-value problem:

$$-\left(\frac{\phi_*'}{\{1+|\phi_*'|^2\}^{\frac{1}{2}}}\right)' + Bo\,\phi_* = Bo\,\overline{V}_c - 2\cos\delta \quad \text{on } (0,1), \tag{2.31}$$

$$\phi_*'(0) = -\operatorname{cotan}\delta, \quad \phi_*'(1) = \operatorname{cotan}\delta, \tag{2.32}$$

$$\overline{V}_c \equiv V_c + \int_0^1 \phi_\Gamma(x_1)\,dx_1 = \int_0^1 \phi_*(x_1)\,dx_1. \tag{2.33}$$

The corresponding static pressure p_* is given by

$$p_* = \frac{1}{Oh^2}(Bo\,\overline{V}_c - 2\cos\delta).$$

The temperature T_* in the static situation is determined by (2.22), (2.24), (2.28) which reduce to:

$$-\frac{1}{Pr}\Delta T_* = 0 \quad \text{in } \Omega_{\phi_*} = \{x \in \mathscr{V} \mid x_2 < \phi_*(x_1)\}, \tag{2.34}$$

$$T_* = h_T \quad \text{on } \Gamma, \tag{2.35}$$

$$-\frac{1}{Pr}\frac{\partial T_*}{\partial \nu} = \frac{Bi_r}{Pr}(T_*^4 - T_{inf}^4) + \frac{Bi_c}{Pr}(T_* - T_{amb})^{1.25} \quad \text{on } S. \tag{2.36}$$

3. Iterative methods; the finite-element method

In this section, we discuss two iterative methods to solve the free-boundary problem (2.20)–(2.30). The first is based on the following principle. A shape is assigned to the free boundary and the flow within that shape is calculated after disregarding one of the boundary conditions on the free boundary. Next, a new free-boundary shape is computed which satisfies as closely as possible the boundary condition that was relaxed. This procedure is repeated until convergence is attained.

The second method also involves a deforming domain but eliminates the successive iteration between the surface position and field variables by introducing, in the discrete case, the position of the nodes on the free surface directly as degrees of freedom. This is then coupled with a quasi-Newton iterative procedure with Broyden's update, which results in the simultaneous calculation of the position of the free surface and the field variables at the new nodal positions once convergence is attained.

The boundary condition on the free surface that will be relaxed in the first iterative method is condition (2.25). Let ϕ be a fixed function satisfying conditions (2.29), (2.30) and belonging to some function space H_ϕ (for a precise definition see Solonnikov 1979). Then an auxiliary problem is defined by finding the solution $\{\boldsymbol{u}, p, T\}$ of problem

(2.20)–(2.24), (2.26)–(2.28). This means that condition (2.25) is relaxed and it is this boundary condition that will be used to adjust the function ϕ.

It can be proved that for small values of Re, Ma and Gr, V_c sufficiently large and $\delta \in (0, \pi)$ the auxiliary problem has a unique solution $\{\boldsymbol{u}, p_0, T\} \in H_u \times H_p \times H_T$ where the pressure p_0 is normalized by

$$\int_{\Omega_\phi} p_0(\boldsymbol{x})\, \mathrm{d}\boldsymbol{x} = 0. \tag{3.1}$$

For precise definitions of H_u, H_p and H_T we refer to Solonnikov (1979). Using (2.29) and (2.30), we deduce from (2.25) that

$$(Oh\ Re)^2 \int_0^1 p(\bar{\boldsymbol{x}})\, \mathrm{d}x_1 = 2\, Oh^2\, Re \int_0^1 \frac{\partial \boldsymbol{u}}{\partial \boldsymbol{v}} \cdot \boldsymbol{v}(\bar{\boldsymbol{x}})\, \mathrm{d}x_1 - 2\cos\delta + Bo\, \bar{V}_c, \tag{3.2}$$

$$\bar{\boldsymbol{x}} = \{x_1, \phi(x_1)\}.$$

When $\{\phi, \boldsymbol{u}, p, T\}$ denotes the solution of the full system (2.20)–(2.30), the pressure p and the pressure p_0 corresponding to the auxiliary problem differ by only a constant, which gives, using (3.1) and (3.2), the following expression for $p(\bar{\boldsymbol{x}})$:

$$\begin{aligned} p(\bar{\boldsymbol{x}}) &= p_0(\bar{\boldsymbol{x}}) + \int_0^1 (p(\bar{\boldsymbol{x}}) - p_0(\bar{\boldsymbol{x}}))\, \mathrm{d}x_1 \\ &= p_0(\bar{\boldsymbol{x}}) - \int_0^1 p_0(\bar{\boldsymbol{x}})\, \mathrm{d}x_1 + \frac{2}{Re} \int_0^1 \frac{\partial \boldsymbol{u}}{\partial \boldsymbol{v}} \cdot \boldsymbol{v}(\bar{\boldsymbol{x}})\, \mathrm{d}x_1 - \frac{2\cos\delta}{(Oh\ Re)^2} + \frac{Bo\, \bar{V}_c}{(Oh\ Re)^2} \\ &= p_0(\bar{\boldsymbol{x}}) + \int_0^1 \sigma_\nu(p_0, \boldsymbol{u})\, (\bar{\boldsymbol{x}})\, \mathrm{d}x_1 - \frac{2\cos\delta}{(Oh\ Re)^2} + \frac{Bo\, \bar{V}_c}{(Oh\ Re)^2}, \end{aligned} \tag{3.3}$$

with

$$\sigma_\nu(p_0, \boldsymbol{u}) = -p_0 + \frac{2}{Re} \frac{\partial \boldsymbol{u}}{\partial \boldsymbol{v}} \cdot \boldsymbol{v}.$$

Substitution of (3.3) into boundary condition (2.25) gives

$$-\frac{1}{R(\phi)} + Bo\, \phi = -(Oh\ Re)^2 \left(\sigma_\nu(p_0, \boldsymbol{u}) - \int_0^1 \sigma_\nu(p_0, \boldsymbol{u})\, \mathrm{d}x_1 \right) - 2\cos\delta + Bo\, \bar{V}_c \quad \text{for } x_1 \in (0, 1). \tag{3.4}$$

The function ϕ will now be compared with the free boundary ϕ_* of the static problem defined by (2.31)–(2.33). Introducing $\psi = \phi - \phi_*$, it can be deduced that ψ satisfies the following nonlinear ordinary differential equation with Neumann-type boundary conditions:

$$\left.\begin{aligned} -\left(\frac{\psi'}{\{1 + |\phi_*'|^2\}^{\frac{1}{2}}} \right)' + Bo\, \psi = G \quad \text{on } (0, 1), \\ \psi'(0) = \psi'(1) = 0, \end{aligned}\right\} \tag{3.5}$$

with G given by

$$\begin{aligned} G = -(Oh\ Re)^2 \left(\sigma_\nu(p_0, \boldsymbol{u}) - \int_0^1 \sigma_\nu(p_0, \boldsymbol{u})\, \mathrm{d}x_1 \right) + \frac{1}{R(\phi)} - \frac{1}{R(\phi_*)} \\ - \left(\frac{\phi' - \phi_*'}{\{1 + |\phi_*'|^2\}^{\frac{1}{2}}} \right)' = G(\phi, \boldsymbol{u}, p_0, T). \end{aligned} \tag{3.6}$$

Next, we define an operator $\mathbf{F}: H_\phi \to H_\phi$ by

$$\mathbf{F}: \hat{\psi} \to \hat{\phi} = \phi_* + \hat{\psi} \to G(\hat{\phi}, \boldsymbol{u}(\hat{\phi}), p_0(\hat{\phi}), T(\hat{\phi})) \overset{(3.5)}{\to} \psi. \tag{3.7}$$

In other words, ψ is the solution of (3.5) where G is replaced by $G(\hat{\phi}, \boldsymbol{u}(\hat{\phi}), p_0(\hat{\phi}), T(\hat{\phi}))$, with $\hat{\phi} = \phi_* + \hat{\psi}$ and $\{\boldsymbol{u}(\hat{\phi}), p_0(\hat{\phi}), T(\hat{\phi})\}$ the unique solution of the auxiliary problem corresponding to $\hat{\phi}$. Using techniques of Solonnikov (1979) the following result can be established: for small values of Re, Ma and Gr, V_c sufficiently large and $\delta \in (0, \pi)$, the operator $\mathbf{F}$ is a contraction in a neighbourhood of the origin of H_ϕ. This proves the existence and uniqueness of the solution $\{\phi, \boldsymbol{u}, p, T\}$ of problem (2.20)–(2.30). The pressure p is calculated from

$$p(\boldsymbol{x}) = p_0(\boldsymbol{x}) + \int_0^1 \left(-p_0(\bar{\boldsymbol{x}}) + \frac{2}{Re} \frac{\partial \boldsymbol{u}}{\partial \boldsymbol{\nu}} \cdot \boldsymbol{\nu}(\bar{\boldsymbol{x}}) \right) \mathrm{d}x_1 + \frac{1}{(Oh\, Re)^2} (Bo\, \bar{V}_c - 2 \cos\delta), \tag{3.8}$$

where p_0 is the normalized pressure of the auxiliary problem corresponding to ϕ.

The algorithm based on these results is the following: the free boundary ϕ is iteratively approximated by a sequence $\phi^0, \phi^1, \ldots, \phi^l$ defined by

(i) $\phi^0 = \phi_*$ static free boundary;
(ii) assume $\phi^1, \phi^2, \ldots, \phi^l$ are known;
(iii) solve the auxiliary problem with ϕ^l; the solution is denoted by $\{\boldsymbol{u}^l, p_0^l, T^l\}$;
(iv) solve problem (3.5) with $G^l = G(\phi^l, \boldsymbol{u}^l, p_0^l, T^l)$; the solution is denoted by ψ^l;
(v) $\phi^{l+1} = \phi_* + \psi^l$. (3.9)

The main steps in the algorithm are the solution of the auxiliary problem (i.e. the Navier–Stokes equations coupled with the heat equation) and the solution of the ordinary differential equation for ψ. The auxiliary problem, which is nonlinear, must be solved iteratively and this can be performed in two different ways. The first, called the coupled method, is to define a sequence $\{\boldsymbol{u}^{l,k}, p_0^{l,k}, T^{l,k}\}_{k=0,1,2,\ldots}$ where $\boldsymbol{u}^{l,k}$, $p_0^{l,k}$ and $T^{l,k}$, $k \geqslant 1$, are computed simultaneously using the quantities $\boldsymbol{u}^{l,k-1}$ and $T^{l,k-1}$ of the previous iteration. When the nonlinear terms are linearized by the Newton–Raphson method, we find the following scheme:

$$\left.\begin{aligned}
&\{\boldsymbol{u}^{l,0}, p_0^{l,0}, T^{l,0}\} = \{\boldsymbol{u}^{l-1}, p_0^{l-1}, T^{l-1}\},\\
&-\frac{1}{Re} \Delta \boldsymbol{u}^{l,k} + (\boldsymbol{u}^{l,k} \cdot \nabla)\, \boldsymbol{u}^{l,k-1} + (\boldsymbol{u}^{l,k-1} \cdot \nabla)\, \boldsymbol{u}^{l,k} + \nabla p_0^{l,k} - \frac{Gr}{Re^2} (T^{l,k} - T_0) \begin{pmatrix} 0 \\ 1 \end{pmatrix}\\
&\qquad = (\boldsymbol{u}^{l,k-1} \cdot \nabla)\, \boldsymbol{u}^{l,k-1}.\\
&\text{Boundary conditions (2.23), (2.26), (2.27) for } \boldsymbol{u}^{l,k}.\\
&\nabla \cdot \boldsymbol{u}^{l,k} = 0,\\
&-\frac{1}{Re\, Pr} \Delta T^{l,k} + (\boldsymbol{u}^{l,k} \cdot \nabla)\, T^{l,k-1} + (\boldsymbol{u}^{l,k-1} \cdot \nabla)\, T^{l,k} = (\boldsymbol{u}^{l,k-1} \cdot \nabla)\, T^{l,k-1}.\\
&\text{Boundary conditions (2.24), (2.28) for } T^{l,k}.
\end{aligned}\right\} \tag{3.10}$$

An alternative method for solving the auxiliary problem is the following uncoupled method which defines a sequence $\{\boldsymbol{u}^{l,k}, p_0^{l,k}, T^{l,k}\}_{k=0,1,\ldots}$ where $\boldsymbol{u}^{l,k}$ and $p_0^{l,k}$, $k \geqslant 1$,

are computed using $\boldsymbol{u}^{l,k-1}$ and $T^{l,k-1}$ with Newton–Raphson linearization for the nonlinear terms and where, next, $\boldsymbol{u}^{l,k}$ is used to compute $T^{l,k}$:

$$\left.\begin{aligned}
&\{\boldsymbol{u}^{l,0}, p_0^{l,0}, T^{l,0}\} = \{\boldsymbol{u}^{l-1}, p_0^{l-1}, T^{l-1}\},\\
&-\frac{1}{Re}\Delta\boldsymbol{u}^{l,k} + (\boldsymbol{u}^{l,k}\cdot\nabla)\,\boldsymbol{u}^{l,k-1} + (\boldsymbol{u}^{l,k-1}\cdot\nabla)\,\boldsymbol{u}^{l,k} + \nabla p_0^{l,k}\\
&\qquad = \frac{Gr}{Re^2}(T^{l,k-1}-T_0)\begin{pmatrix}0\\1\end{pmatrix} + (\boldsymbol{u}^{l,k-1}\cdot\nabla)\,\boldsymbol{u}^{l,k-1}.\\
&\text{Boundary conditions (2.23), (2.26), (2.27) for } \boldsymbol{u}^{l,k}\\
&\qquad\qquad \nabla\cdot\boldsymbol{u}^{l,k} = 0,\\
&\qquad -\frac{1}{Re\,Pr}\Delta T^{l,k} + (\boldsymbol{u}^{l,k}\cdot\nabla)\,T^{l,k} = 0,\\
&\text{Boundary conditions (2.24), (2.28) for } T^{l,k}.
\end{aligned}\right\} \tag{3.11}$$

For both schemes (3.10) and (3.11), the Newton–Raphson linearization of boundary condition (2.28) reads

$$\begin{aligned}
-\frac{1}{Re\,Pr}\frac{\partial T^{l,k}}{\partial \nu} = \frac{Bi_r}{Re\,Pr}\{4(T^{l,k-1})^3\,T^{l,k} - 3(T^{l,k-1})^4 - T_{\text{inf}}^4\}\\
+\frac{Bi_c}{Re\,Pr}\{1.25(T^{l,k-1}-T_{\text{amb}})^{0.25}(T^{l,k}-T^{l,k-1})\\
+(T^{l,k-1}-T_{\text{amb}})^{1.25}\}.
\end{aligned}$$

We define

$$\{\boldsymbol{u}^l, p_0^l, T^l\} = \lim_{k\to\infty}\{\boldsymbol{u}^{l,k}, p_0^{l,k}, T^{l,k}\}.$$

Results on the existence and uniqueness of a solution $\{\boldsymbol{u}^l, p_0^l, T^l\}$ of the auxiliary problem and the convergence of the iterative methods (3.10), (3.11) can be found in Driessen (1984).

Once $\{\boldsymbol{u}^l, p_0^l, T^l\}$ is known, we calculate $G(\phi^l, \boldsymbol{u}^l, p_0^l, T^l)$ and we solve problem (3.5) which has a unique solution for $Bo \geqslant 0$. Indeed, (3.5) is an elliptic boundary-value problem with Neumann boundary conditions, the solution of which must satisfy

$$\int_0^1 \psi(x_1)\,\mathrm{d}x_1 = 0.$$

Both methods have been discretized using the (triangular) finite-element method in combination with a penalty method for the incompressibility constraint. For the velocity we have chosen continuous piecewise extended-quadratic basis functions based on 7 points (three vertices, three midpoints of edges and the centroid) together with piecewise-linear non-continuous basis functions for the pressure (see Crouzeix & Raviart 1973). The velocities in the centroid of each triangle have been eliminated with the aid of the continuity equation. The temperature is approximated by a full quadratic polynomial in each element based on six points (three vertices, three mid-points of sides). The function ϕ is approximated by a one-dimensional quadratic element. For an introduction to the finite-element method and applications to the Navier–Stokes equations we refer to Cuvelier, Segal & van Steenhoven (1986).

Numerical experiments will be shown in §4. We note that the uncoupled method

(3.11) requires less memory than the coupled method (3.10) but its convergence rate is linear, whereas the coupled method converges quadratically. Nevertheless, the convergence of the sequence $\{\phi^l, \boldsymbol{u}^l, p_0^l, T^l\}$ is linear irrespective of which inner-iteration, (3.10) or (3.11), is used.

The following method, which is in some sense related to the coupled method (3.10), is based on the simultaneous calculation of the position of the free surface and the field variables. The procedure is as follows. Using the finite-element method, a large system of (nonlinear) equations is constructed where the field variables (i.e. velocity, pressure and temperature) as well as the position of the nodes of the free surface are considered as degrees of freedom. This large system will be solved by Newton's method or a quasi-Newton method using a Broyden update for the inverse of the Jacobian of the system. Let us construct the large system of equations, which are in fact the Galerkin finite-element equations. We first write the not yet discretized Galerkin equations, which are obtained by multiplying (2.20), (2.21), (2.22) and (2.25) by appropriate test functions, taking the integral over the corresponding domain and substitution of boundary conditions.

The momentum equation (2.20) is multiplied by a test (vector-) function $\boldsymbol{v} = \{v_1, v_2\}$ satisfying $\boldsymbol{v} = 0$ on Γ and $v_\nu = 0$ on S. Integration over Ω_ϕ, application of Green's formula and substitution of the boundary conditions (2.23), (2.26) and (2.27) leads to

$$a(\boldsymbol{u}, \boldsymbol{v}) + b(\boldsymbol{u}, \boldsymbol{w}, \boldsymbol{v}) - (p_0, \nabla\cdot\boldsymbol{v})_{\Omega_\phi} - \frac{Gr}{Re^2}(T - T_0, v_2)_{\Omega_\phi} + \frac{Ma}{Re^2\,Pr}\left(\frac{\partial T}{\partial \tau}, v_\tau\right)_\phi = 0, \quad (3.12)$$

where

$$a(\boldsymbol{u}, \boldsymbol{v}) = \frac{1}{2Re}\sum_{i,j=1}^{2}\int_{\Omega_\phi}\left(\frac{\partial u_i}{\partial x_j} + \frac{\partial u_j}{\partial x_i}\right)\left(\frac{\partial v_i}{\partial x_j} + \frac{\partial v_j}{\partial x_i}\right)\mathrm{d}\boldsymbol{x},$$

$$b(\boldsymbol{u}, \boldsymbol{w}, \boldsymbol{v}) = \sum_{i,j=1}^{2}\int_{\Omega_\phi} u_i \frac{\partial w_j}{\partial x_i} v_j \,\mathrm{d}\boldsymbol{x},$$

$$(\boldsymbol{v}, \boldsymbol{w})_{\Omega_\phi} = \int_{\Omega_\phi} \boldsymbol{v}\cdot\boldsymbol{w}\,\mathrm{d}\boldsymbol{x},$$

$$(\boldsymbol{v}, \boldsymbol{w})_\phi = \int_S \boldsymbol{v}\cdot\boldsymbol{w}\,\mathrm{d}S.$$

The incompressibility constraint (2.21) is multiplied by a test function q, which gives, after integration over Ω_ϕ,

$$(q, \nabla\cdot\boldsymbol{u})_{\Omega_\phi} = 0. \quad (3.13)$$

The energy equation (2.22) is multiplied by a test function θ satisfying $\theta = 0$ on Γ. Integration over Ω_ϕ, application of Green's formula and substitution of (2.24), (2.28) gives

$$\tilde{a}(T, \theta) + \tilde{b}(\boldsymbol{u}, T, \theta) + \left(\frac{Bi_r}{Re\,Pr}(T^4 - T_{\mathrm{inf}}^4) + \frac{Bi_c}{Re\,Pr}(T - T_{\mathrm{amb}})^{1.25}, \theta\right)_\phi = 0, \quad (3.14)$$

with

$$\tilde{a}(T, \theta) = \frac{1}{Re\,Pr}\sum_{i=1}^{2}\int_{\Omega_\phi}\frac{\partial T}{\partial x_i}\frac{\partial \theta}{\partial x_i}\,\mathrm{d}\boldsymbol{x},$$

$$\tilde{b}(\boldsymbol{u}, T, \theta) = \sum_{i=1}^{2}\int_{\Omega_\phi} U_i \frac{\partial T}{\partial x_i}\theta\,\mathrm{d}\boldsymbol{x}.$$

Finally we multiply (3.4), which is equivalent to (2.25), by a test function χ, integrate from 0 to 1, apply Green's formula and substitute the boundary conditions (2.29) to obtain

$$\int_0^1 \frac{\phi'}{\{1+|\phi'|^2\}^{\frac{1}{2}}}\chi' \,\mathrm{d}x_1 + Bo\int_0^1 \phi\chi \,\mathrm{d}x_1 = -(Oh\ Re)^2 \int_0^1 \left\{\sigma_\nu(p_0, \boldsymbol{u})\,\chi - \chi\int_0^1 \sigma_\nu(p_0, \boldsymbol{u})\,\mathrm{d}x_1\right\}\mathrm{d}x_1$$
$$+ (Bo\ \overline{V}_c - 2\cos\delta)\int_0^1 \chi \,\mathrm{d}x_1 + (\chi(0)+\chi(1))\cos\delta. \tag{3.15}$$

Next, we discretize (3.12), (3.13), (3.14), (3.15) using a (triangular) finite-element method. The velocity (i.e. $\boldsymbol{u}$ and v) is approximated by continuous piecewise extended-quadratic polynomials. The pressure (i.e. p_0 and q) is approximated by piecewise-linear polynomials not necessarily continuous in Ω. The temperature (i.e. T and θ) is approximated by a continuous piecewise-quadratic polynomial. Finally, we approximate the free boundary (i.e. ϕ and χ) by continuous piecewise quadratic one-dimensional polynomials. The finite-element approximation of all quantities is indicated by an index h. Since the basis functions q_h are discontinuous, the discretized form of (3.13) is equivalent to

$$\int_e \nabla\cdot\boldsymbol{u}_h \,\mathrm{d}\boldsymbol{x} = 0, \tag{3.16}$$

$$\int_e (x_1 - a_1^7)\,\nabla\cdot\boldsymbol{u}_h \,\mathrm{d}\boldsymbol{x} = 0, \quad \int_e (x_2 - a_2^7)\,\nabla\cdot\boldsymbol{u}_h \,\mathrm{d}\boldsymbol{x} = 0, \tag{3.17}$$

for each triangle e, where $\{a_1^7, a_2^7\}$ denotes the centroid of e. The relations (3.17) are used to eliminate the velocity unknowns in the centroid, so that the velocity on each triangle e is determined by the values in six points (three vertices and three mid-points of edges). Relation (3.16) will be satisfied in the following penalized way. We replace (3.16) by

$$\epsilon(p_{0h}, q_h)_{\Omega_\phi} + (q_h, \nabla\cdot\boldsymbol{u}_h)_{\Omega_\phi} = 0 \quad (\epsilon > 0 \text{ small parameter}) \tag{3.18}$$

for all piecewise constant functions q_h.

This finite-element approximation results in a matrix system of nonlinear algebraic equations of the form

$$(3.12)_h: \quad \boldsymbol{A}\boldsymbol{u}_h + \boldsymbol{B}(\boldsymbol{u}_h)\,\boldsymbol{u}_h + \boldsymbol{C}\boldsymbol{p}_{0h} + \boldsymbol{D}\boldsymbol{T}_h = \boldsymbol{F}, \tag{3.19}$$

$$(3.18)_h: \quad \epsilon\boldsymbol{M}\boldsymbol{p}_{0h} + \boldsymbol{C}^{\mathrm{T}}\boldsymbol{u}_h = 0, \tag{3.20}$$

$$(3.14)_h: \quad \tilde{\boldsymbol{A}}\boldsymbol{T}_h + \tilde{\boldsymbol{B}}(\boldsymbol{u}_h)\,\boldsymbol{T}_h = \boldsymbol{G}, \tag{3.21}$$

$$(3.15)_h: \quad \boldsymbol{K}\boldsymbol{\phi}_h + \boldsymbol{L}\boldsymbol{u}_h + \boldsymbol{N}\boldsymbol{p}_{0h} = \boldsymbol{H}, \tag{3.22}$$

where $\boldsymbol{u}_h$, $\boldsymbol{p}_{0h}$, $\boldsymbol{T}_h$ and $\boldsymbol{\phi}_h$ are the vector representations of $\boldsymbol{u}_h$, p_{0h}, T_h and ϕ_h respectively. Notice also that the matrices $\boldsymbol{A}, \boldsymbol{B}, \boldsymbol{C}, \boldsymbol{D}, \boldsymbol{M}, \boldsymbol{C}^{\mathrm{T}}, \tilde{\boldsymbol{A}}, \tilde{\boldsymbol{B}}, \boldsymbol{K}, \boldsymbol{L}, \boldsymbol{N}$ and the vectors $\boldsymbol{F}$, $\boldsymbol{G}$, and $\boldsymbol{H}$ all depend on ϕ_h through the integration over Ω_ϕ which depends on ϕ_h.

If the vector $\boldsymbol{p}_{0h}$ is eliminated from system (3.19)–(3.22), we obtain the reduced system

$$\begin{bmatrix} \boldsymbol{A}+\boldsymbol{B}(\boldsymbol{u}_h)-\frac{1}{\epsilon}\boldsymbol{C}\boldsymbol{M}^{-1}\boldsymbol{C}^{\mathrm{T}} & \boldsymbol{D} & 0 \\ 0 & \tilde{\boldsymbol{A}}+\tilde{\boldsymbol{B}}(\boldsymbol{u}_h) & 0 \\ \boldsymbol{L}-\frac{1}{\epsilon}\boldsymbol{N}\boldsymbol{M}^{-1}\boldsymbol{C}^{\mathrm{T}} & 0 & \boldsymbol{K} \end{bmatrix} \begin{bmatrix} \boldsymbol{u}_h \\ \boldsymbol{T}_h \\ \boldsymbol{\phi}_h \end{bmatrix} = \begin{bmatrix} \boldsymbol{F} \\ \boldsymbol{G} \\ \boldsymbol{H} \end{bmatrix}, \tag{3.23}$$

which we write in abbreviated form as

$$\boldsymbol{S}(\boldsymbol{w})\,\boldsymbol{w} = \boldsymbol{s}(\boldsymbol{w}), \quad \boldsymbol{w} = \{\boldsymbol{u}_h, T_h, \phi_h\}. \tag{3.24}$$

The Newton–Raphson algorithm for solving this system can be written as:

(i) let $\boldsymbol{w}^0$ be an approximation of the solution $\boldsymbol{w}$; (ii) assume $\boldsymbol{w}^1, \boldsymbol{w}^2, \ldots, \boldsymbol{w}^l$ are known; (iii) $\boldsymbol{w}^{l+1}$ is defined as the solution of the following system of (linear) algebraic equations:

$$\boldsymbol{J}(\boldsymbol{w}^l)\,\boldsymbol{w}^{l+1} = \boldsymbol{J}(\boldsymbol{w}^l)\,\boldsymbol{w}^l - (\boldsymbol{S}(\boldsymbol{w}^l)\,\boldsymbol{w}^l - \boldsymbol{s}(\boldsymbol{w}^l)) \tag{3.25}$$

where $\boldsymbol{J}(\boldsymbol{w}) = \partial\,\mathrm{Res}\,(\boldsymbol{w})/\partial \boldsymbol{w}$, $\mathrm{Res}\,(\boldsymbol{w}) = \boldsymbol{S}\boldsymbol{w} - \boldsymbol{s}$, is the Jacobian matrix of (3.24). When we write (3.25) explicitly we observe that the partitioned upper-left-hand corner matrix, i.e. the system corresponding to a fixed domain, is identical to the discretization of (3.10) using the same finite element for u_h and T_h and the same penalization for the incompressibility constraint.

The Newton–Raphson method (3.25) requires at each iteration step the computation, assembly and factorization of the Jacobian matrix. In order to reduce this cost, we use a quasi-Newton method for which only an initial Jacobian is assembled and factorized. Next, for each subsequent iteration this matrix is updated in a cost-effective way. The algorithm we have used is the quasi-Newton method with Broyden's update:

(i) let $\boldsymbol{w}^0$ be an approximation of $\boldsymbol{w}$;

(ii) assemble $\boldsymbol{J}(\boldsymbol{w}^0)$;

(iii) factorize $\boldsymbol{H}_0^{-1} \equiv \boldsymbol{J}^{-1}(\boldsymbol{w}^0)$;

(iv) $\boldsymbol{w}^1 = \boldsymbol{H}_0^{-1}\,\boldsymbol{w}^0, \ldots, \boldsymbol{w}^l = \boldsymbol{H}_{l-1}^{-1}\,\boldsymbol{w}^{l-1}$;

(v) $$\boldsymbol{H}_l^{-1} = \boldsymbol{H}_{l-1}^{-1} + \frac{(\alpha_l - \boldsymbol{H}_{l-1}^{-1}\beta_l)\,\alpha_l^{\mathrm{T}}}{\alpha_l\,\boldsymbol{H}_{l-1}^{-1}\beta_l}\,\boldsymbol{H}_{l-1}^{-1};$$

with

$$\alpha_l = \boldsymbol{w}^l - \boldsymbol{w}^{l-1}, \quad \beta_l = \mathrm{Res}\,(\boldsymbol{w}^l) - \mathrm{Res}\,(\boldsymbol{w}^{l-1})$$

(vi) $\boldsymbol{w}^{l+1} = \boldsymbol{H}_l^{-1}\,\boldsymbol{w}^l$. (3.26)

$\boldsymbol{H}_l = \boldsymbol{J}(\boldsymbol{w}^l) + O(\alpha_l)$ and the convergence rate approaches a Newton–Raphson one, while the cost of one iteration is drastically reduced. For a complete description of quasi-Newton's method with Broyden's update the reader is referred to Dennis & More (1977). Application of this technique to the case of a fixed domain can be found in Engelman, Strang & Bathe (1981); for applications to an isothermal free-boundary problem we refer to Kistler & Scriven (1984), Ruschak (1980) and Saito & Scriven (1981).

4. Numerical experiments

In order to determine some of the characteristics of the iterative methods discussed in the preceding section, we apply these methods to a model problem of floating-zone open-boat type. In particular we compare the convergence behaviour of the three methods and study the influence of the characteristic numbers *Gr*, *Pr*, *Ma*, *Bo*, *Oh*, Bi_r and Bi_c on the shape of the free boundary. The computations were performed on the Amdahl 470 V/7-B computer at the Delft University of Technology. The

program was constructed with aid of A Finite-Element Package (AFEP) (see Segal 1979) and FIDAP fluid dynamics analysis package (see Engelman 1984). These packages consist of a number of subroutines for solving partial differential equations with the finite-element method.

The model problem is a free-boundary variant of the generally accepted problem (see Jones & Thomson 1981) that is used to compare and to test computer codes for the solution of the Boussinesq equations. In normalized quantities $\mathscr{V}$ is defined by

$$\mathscr{V} = \{\{x_1, x_2\} \in \mathbb{R}^2 \mid 0 < x_1 < 1,\ x_2 > 0\}$$

and the quantity of fluid (or melt) contained in $\mathscr{V}$ is equal to unity. For the velocity we assume that the no-slip condition is satisfied on the boundary of the container. This implies $\boldsymbol{h}_u \equiv 0$, so that the velocity scale U can be chosen such that $Re = 1$. The vertical boundaries of the region at $x_1 = 0$ and $x_1 = 1$ (which can be interpreted as the crucible wall and the melt–crystal interface, cf. §2) have normalized temperature equal to $T_0 + \frac{1}{2}$ and $T_0 - \frac{1}{2}$ respectively, while at the horizontal boundary at $x_2 = 0$ the temperature is linear: $T = T_0 + \frac{1}{2} - x_1$. For all numerical experiments we fixed the contact angle at 90°, which means that the region occupied by the melt in the static situation (i.e. $Gr = 0, Ma = 0$) is given by $\Omega_{\phi_*} = \{\{x_1, x_2\} \in \mathbb{R}^2 \mid 0 < x_1, < 1, 0 < x_2 < 1\}$ and $\phi_* \equiv 1$. The corresponding temperature for $Bi_r = 0$ and $Bi_c = 0$ satisfies $T_* = T_0 + \frac{1}{2} - x_1$. On the region Ω_{ϕ_*} we used a regular triangulation which corresponds to a space discretization of $\Delta x_1 = \Delta x_2 = 0.05$. The number of triangular elements was equal to 200, the number of line elements was 10. The numerical experiments are performed for the following range of the characteristic numbers: $-2.10^4 \leqslant Gr \leqslant 10^5$, $0.73 \leqslant Pr \leqslant 219$, $0.0 \leqslant Ma \leqslant 400$, $0.0 \leqslant Bo \leqslant 10^3$, $5.10^{-3} \leqslant Oh \leqslant 1.0$, without radiation and cooling ($Bi_r = 0$, $Bi_c = 0$). Numerical results for radiation ($Bi_r = 2 \times 10^{-4}$) and cooling ($Bi_c = 0.4$) will be shown in figures 11(*e–l*). We applied method 1 (algorithm (3.9), (3.10)), method 2 (algorithm (3.9), (3.11)) and method 3 (algorithm (3.26)) to the model problem. The computations are terminated when the difference between two successive free boundaries is smaller than 10^{-3}. The inner-iterations (3.10) in method 1 and (3.11) in method 2 are terminated when the difference in temperature as well as the difference in velocity of two successive iterations is smaller than a tolerance of 10^{-5}. This tolerance is kept small in order to control the convergence behaviour of the inner-iteration. For practical computations one or two inner-iterations are sufficient in many cases.

In our computations we observed the following convergence behaviour. Algorithm (3.9) has a linear convergence rate, irrespective of the choice of the inner-iteration (3.10) or (3.11). The convergence rate of method 3 is almost quadratic (superlinear). The inner-iteration (3.10), which couples the velocity and the temperature for a fixed domain, has a quadratic convergence rate. The inner-iteration (3.11), which iterates between the velocity and the temperature for a fixed domain, has a quadratic convergence rate for low Prandtl numbers, otherwise it is a linear process. For all the iterative processes it is essential that a first guess is made in the neighbourhood of the solution. For moderate values of Gr and Ma the static solution can serve as a start for the algorithm. For large values of Gr and Ma a good start is given by the solution of a situation for a lower Grashof or Marangoni number. To illustrate these convergence properties we give in table 1 the differences of two successive free boundaries for the situation with $Gr = 600$, $Pr = 0.73$, $Ma = 0$, $Bo = 0$, $Oh = 0.1$. In columns 2–3 and 5–6 the inner-iteration accuracy for method 1 and 2 equals 10^{-5}; in columns 4 and 7 only one inner-iteration is performed for method 1 and 2.

In particular, method 3 needs starting values in the close neighbourhood of the

	Method 1			Method 2			
Outer iterations	Inner iterations	Accuracy	1 inner-iteration accuracy	Inner-iterations	Accuracy	1 inner-iteration accuracy	Method 3 accuracy
$l = 1$	5	0.12 (0)	0.14 (0)	9	0.12 (0)	0.13 (0)	0.14 (0)
2	4	0.23 (−1)	0.15 (−1)	8	0.23 (−1)	0.12 (−1)	0.22 (−1)
3	3	0.10 (−1)	0.13 (−1)	7	0.10 (−1)	0.13 (−1)	0.45 (−2)
4	2	0.56 (−2)	0.56 (−2)	7	0.56 (−2)	0.54 (−2)	0.24 (−4)
5	2	0.34 (−2)	0.33 (−2)	6	0.34 (−2)	0.33 (−2)	
6	2	0.17 (−2)	0.16 (−2)	4	0.17 (−2)	0.19 (−2)	
7	1	0.92 (−3)	0.92 (−3)	3	0.92 (−3)	0.12 (−2)	
8	—	—	—	—	—	0.87 (−3)	

TABLE 1. Outer-iterations, inner-iterations and accuracy $\max|\phi^l - \phi^{l-1}|$ for $Gr = 600$, $Pr = 0.73$, $Ma = 0$, $Bo = 0$, $Oh = 0.1$, $Bi_r = 0$, $Bi_c = 0$. $a(b)$ means $a * 10^b$.

Figure	Gr	Pr	Ma	Bo	Oh	Bi_r	Bi_c	$\|u\|$	$\phi(0)$	$\phi(1)$
5(*a*)	2.0	0.73	0	0	1.0	0	0	0.0125	1.021	0.978
5(*b*)	14.0	0.73	0	0	1.0	0	0	0.0785	1.204	0.773
5(*c*)	2.0	0.73	0	0	0.1	0	0	0.0125	1.000	1.000
5(*d*)	1200	0.73	0	0	0.1	0	0	5.92	1.163	0.816
5(*e*)	2.0	0.73	0	0	0.01	0	0	0.0125	1.000	1.000
5(*f*)	2×10^4	0.73	0	0	0.01	0	0	40.0	1.009	0.992
5(*g*)	200	0.73	0	0	0.005	0	0	1.24	1.000	1.000
5(*h*)	10^5	0.73	0	0	0.005	0	0	87.2	1.007	0.995
6(*a*)	14.0	21.9	0	0	1.0	0	0	0.0734	1.221	0.752
6(*b*)	14.0	219	0	0	1.0	0	0	0.0438	1.175	0.800
7(*a*)	1200	0.73	0	1.0	0.1	0	0	6.10	1.135	0.850
7(*b*)	1200	0.73	0	1000	0.1	0	0	6.77	1.001	0.999
8(*a*)	0	0.73	0.5	0	1.0	0	0	0.0952	0.944	1.063
8(*b*)	0	0.73	2.5	0	1.0	0	0	0.418	0.567	1.488
8(*c*)	0	0.73	50	0	0.1	0	0	8.85	0.942	1.077
8(*d*)	0	0.73	150	0	0.1	0	0	19.1	0.642	1.492
8(*e*)	0	0.73	50	0	0.01	0	0	9.12	1.000	1.001
8(*f*)	0	0.73	400	0	0.01	0	0	40.3	0.998	1.003
9(*a*)	0	0.73	100	0	0.1	0	0	15.0	0.849	1.219
9(*b*)	0	0.73	100	1.0	0.1	0	0	15.2	0.870	1.195
9(*c*)	0	0.73	100	1000	0.1	0	0	16.7	0.999	1.002
10(*a*)	−200	0.73	50	0	0.1	0	0	7.76	0.919	1.097
10(*b*)	−800	0.73	50	0	0.1	0	0	4.99	0.827	1.177
10(*c*)	−1000	0.73	50	0	0.1	0	0	4.61	0.768	1.229
10(*d*)	−1500	0.73	50	0	0.01	0	0	5.43	0.998	1.002
10(*e*)	-2×10^4	0.73	300	0	0.01	0	0	34.3	0.983	1.015
11(*a*)	2×10^4	0.73	146	1000	0.1	0	0	43.1	1.010	0.973
11(*b*)	2000	0.73	146	100	0.1	0	0	28.4	1.012	0.954
11(*c*)	200	0.73	146	10	0.1	0	0	21.3	0.903	1.204
11(*d*)	20	0.73	146	1.0	0.1	0	0	19.6	0.723	1.414
11(*e*)	2×10^4	0.73	146	1000	0.1	2×10^{-4}	0	51.1	1.014	0.988
11(*f*)	2000	0.73	146	100	0.1	2×10^{-4}	0	27.0	1.007	1.040
11(*g*)	200	0.73	146	10	0.1	2×10^{-4}	0	23.0	0.946	1.159
11(*h*)	20	0.73	146	1.0	0.1	2×10^{-4}	0	22.2	0.830	1.300
11(*i*)	2×10^4	0.73	146	1000	0.1	0	0.4	50.0	1.013	0.986
11(*j*)	2000	0.73	146	100	0.1	0	0.4	26.7	1.006	1.039
11(*k*)	200	0.73	146	10	0.1	0	0.4	22.6	0.939	1.165
11(*l*)	20	0.73	146	1.0	0.1	0	0.4	22.1	0.817	1.311

TABLE 2. Data for figures 5–11.

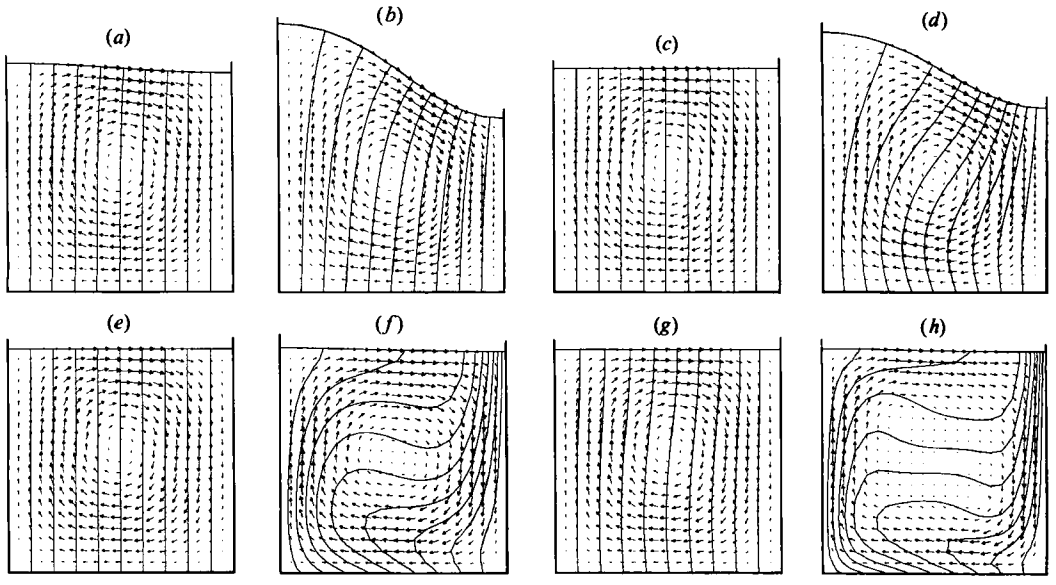

FIGURE 5. The influence of the Grashof number on the shape of the free boundary, the temperature distribution and the flow field: parameters given in table 2.

final solution. Moreover method 3 requires more computer storage than method 1, which, in turn, requires more memory than method 2. When all three methods do converge, they converge to the same (unique) solution of the free-boundary problem.

In the figures we show the velocity vectors in the nodal points of the triangulation and the isotherms. The velocity vectors are scaled, the maximum velocity $|\boldsymbol{u}|$ is indicated for each figure. The isotherms are given for $T = T_0+\frac{1}{2}$ to $T = T_0-\frac{1}{2}$ with increments of 0.1. For each figure we also give the values of $\phi(0)$ and $\phi(1)$ for the height of the free boundary at $x_1 = 0$ and $x_1 = 1$. Data corresponding to figures 5–11 are given in table 2.

The Grashof number represents the relative importance of the buoyancy forces with respect to the viscous forces. The influence of this number on the shape of the free boundary, the temperature distribution and the flow field is shown in figure 5(*a–h*) for $Pr = 0.73$, $Ma = 0$, $Bo = 0$ and different values of the Ohnesorge number ranging from $Oh = 1.0$ to 0.005. Since the Grashof number appears on the right-hand side of the second component of the Navier–Stokes equations, the corresponding buoyancy force acts on the fluid particles in an upward direction near the left-hand vertical boundary (i.e. where $T = T_0+\frac{1}{2}$) and acts downwards near the right-hand vertical boundary, where $T = T_0-\frac{1}{2}$. This imbalance of forces induces an overpressure in the left upper corner and an underpressure in the right upper corner of the melt region. This causes the free boundary to rise near $x_1 = 0$ and to drop near $x_1 = 1$. When we choose $Gr > 14.0$ for $Oh = 1.0$ or $Gr > 1200$ for $Oh = 0.1$ the iterative methods do not converge, because the finite-element triangulation becomes too distorted with respect to the initial triangulation. For $Oh = 0.01$ and $Gr > 2.10^4$ or $Oh = 0.005$ and $Gr > 10^5$ none of the methods 1, 2 or 3 converge. In general, for large values of the Grashof number, the convective terms in the Navier–Stokes equations dominate the diffusive terms and a finer grid is necessary in order to take into account the velocity boundary layer near the vertical walls. From the numerical results the order of magnitude of the velocity $\boldsymbol{u}$ and the pressure p can be estimated from $|\boldsymbol{u}| \sim Gr^{\frac{1}{2}}$, $p \sim Gr$ for large

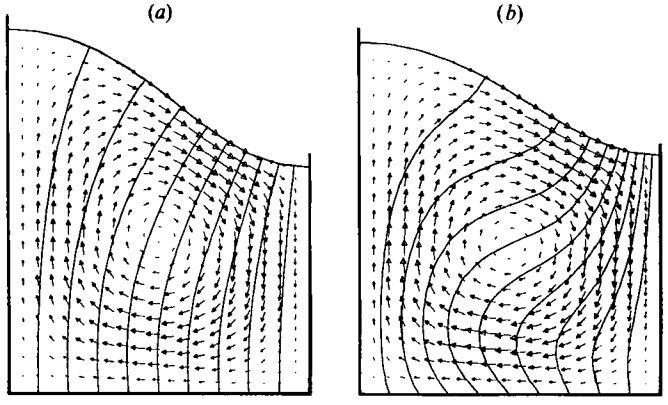

FIGURE 6. The influence of the Prandtl number on the shape of the free boundary, the temperature distribution and the flow field: parameters given in table 2.

values of Gr, whereas for small Grashof numbers $|\boldsymbol{u}| \sim Gr$, $p \sim Gr$. This agrees with estimates given in Ostrach (1982). These estimates are practically independent of the Ohnesorge number. The rise $\Delta\phi$ in the free boundary for $Bo = 0$ can be obtained from (2.25) and the estimate for p: $\Delta\phi \sim Gr\,Oh^2$. The influence of the Prandtl number, which gives the ratio of viscous forces to thermal forces, is shown in figures 5(*a*), 6(*a*, *b*), where the temperature distribution and flow are depicted for $Pr = 0.73$, 21.9, 219.0 respectively and $Gr = 14.0$, $Oh = 1.0$, $Bo = 0$, $Ma = 0$.

For melts with low Prandtl numbers (such as molten metals), the temperature distribution is almost independent of the flow, because heat is mainly transported by conduction. For melts with high Prandtl numbers, such as molten oxides, the convective heat transfer becomes more significant and the isotherms become more distorted than those of pure conduction. This causes a change in the flow field which can be seen from a decrease of the magnitude of the velocity vector and a flattening of the free surface. Nevertheless, the influence of the Prandtl number on the shape of the free boundary is small. When the Rayleigh Number $Ra = Gr\,Pr$ is large, a thermal boundary layer appears along the crystal–melt interfaces. In this case, the fluid becomes isothermal (i.e. $T = T_0$), except in the boundary layers. The influence of the Bond number, which indicates the importance of gravitation versus capillary forces, in a pure Grashof convection problem (i.e. when $Ma = 0$) can be studied from the experiments corresponding to figures 5(*d*), 7(*a*, *b*).

These figures give the results for $Gr = 1200$, $Pr = 0.73$, $Ma = 0$, $Oh = 0.1$ and $Bo = 0$, 1.0, 10^3. We observe that increasing the Bond number has a flattening effect on the free boundary, while the velocity field and the temperature distribution are hardly changed (comparing the values at corresponding nodal points of the finite-element triangulation) when Bo varies between 0 and 10^3. The stabilizing effect of the Bond number was studied in Cuvelier (1985) where it was found that the damping factor of a small perturbation increases with the Bond number. When the Bond number tends to infinity (i.e. $Bo \approx 10^3$ corresponding to terrestrial conditions), (3.4) can be considered as a singularly perturbed second-order equation. The term $Bo\,\phi$ dominates the term $1/R(\phi)$. It is well known (cf. Lions 1973) that the solution of equations of this type is almost constant in the interior of (0, 1) and satisfies the boundary conditions at $x_1 = 0$ and 1. For (3.4) this means $\phi \approx \overline{V}_c = 1$ on (0, 1) (cf. figure 7*b*).

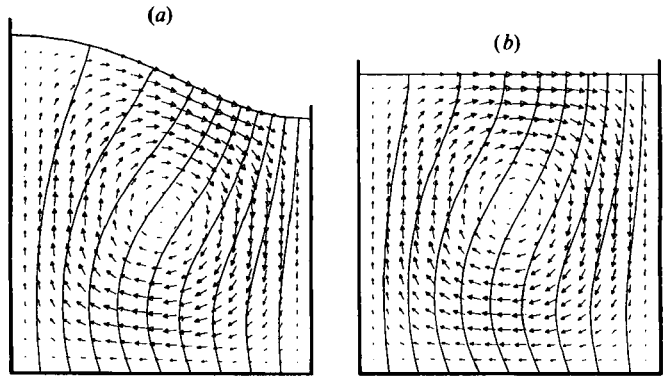

FIGURE 7. The influence of the Bond number on the shape of the free boundary, the temperature distribution and the flow field: parameters given in table 2.

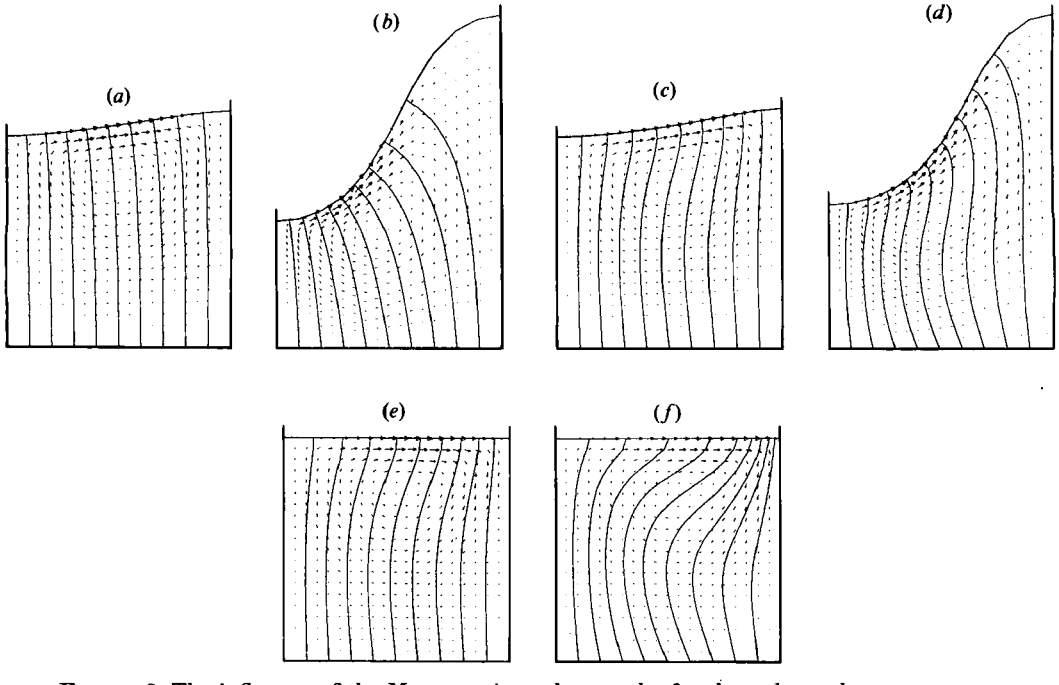

FIGURE 8. The influence of the Marangoni number on the free boundary, the temperature distribution and the flow field: parameters given in table 2.

Since the Grashof number appears in the right-hand side of the Navier–Stokes equations, the Grashof convection is a typical bulk-flow phenomenon. The buoyancy force acts as a body force on the fluid as a whole. On the other hand, the Marangoni number appears in the tangential-stress boundary condition, which gives rise to a shear stress on the free boundary of the melt. This surface force induces the so-called Marangoni (or thermocapillary) convection, which is a typical surface phenomenon. This phenomenon is shown in figures 8 (*a–f*) where the free boundary, the temperature distribution and the velocity vectors are given for $Gr = 0$, $Pr = 0.73$, $Bo = 0$, $Oh = 1.0, 0.1, 0.01$ and various values of the Marangoni number.

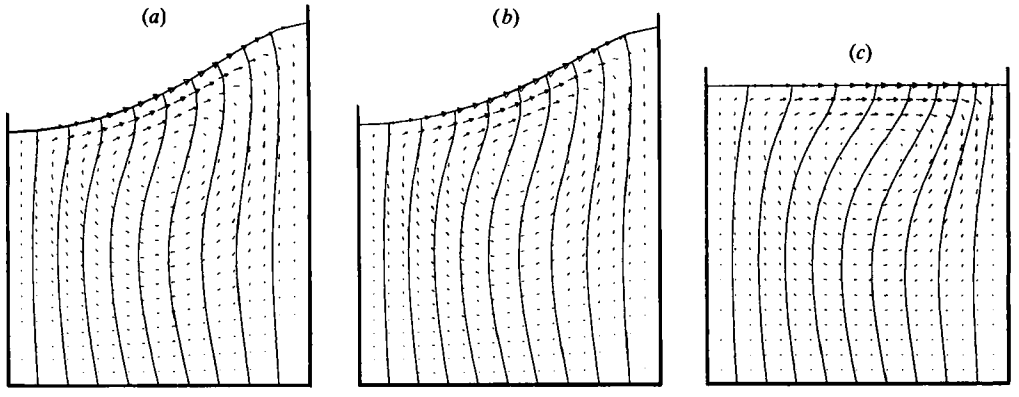

FIGURE 9. The variation of the free boundary, the temperature distribution and the flow field with Bond number: parameters given in table 2.

The shear stress on the free boundary causes a build-up in the pressure in the upper-right corner of the melt, which results in an overpressure near the cold wall and an underpressure near the hot wall. Consequently the free boundary is higher at $x_1 = 1$ and lower at $x_1 = 0$. The vorticity sources on the free boundary diffuse into the interior of the flow field, resulting in one vortex whose centre is situated near the free boundary. The order of magnitude of the velocity $\boldsymbol{u}$ can be estimated from $|\boldsymbol{u}| \sim Ma$ for small values of Ma, while for large Marangoni numbers $|\boldsymbol{u}| \sim (Ma)^{\frac{2}{3}}$ (see Ostrach 1982). The iterative methods do not converge when the mesh becomes too distorted, i.e. when the free boundary is too far away from the static solution. The solution procedure for the Navier–Stokes equations in a fixed domain fails to converge when the convective terms dominate the diffusive terms, i.e. when the velocity becomes too large. In this case mesh refinement is necessary. The maximum rise $\Delta\phi$ of the free boundary with respect to the static solution is estimated from $\Delta\phi \sim Ma\, Oh^2$. For small values of the Marangoni number there is little thermal convection, which implies that the temperature distribution is essentially determined by conduction. For large values of Oh, for instance $Oh \approx 1.0$, this gives a large surface-temperature gradient near $x_1 = 0$ (see figure 8*b*), while for small Oh, $Oh \approx 0.01$, a large surface-temperature gradient is observed near $x_1 = 1$. For large Marangoni numbers convection dominates the diffusion. The flow brings hotter fluid towards the cold wall at $x_1 = 1$, resulting into a large surface-temperature gradient near $x_1 = 1$ for small Ohnesorge numbers (see figure 8*f*). The large vorticity sources created by this surface-temperature gradient diffuse into the flow field and accelerate the fluid locally. For large Marangoni numbers a shift of the centre of the vortex towards the cold wall is observed.

Figures 9(*a*, *b*, *c*) show the flow pattern for $Gr = 0$, $Pr = 0.73$, $Ma = 100$, $Oh = 0.1$ and various values of the Bond number. Concerning the influence of the Bond number on pure Marangoni convection, i.e. when $Gr = 0$, the same remarks apply as for its influence on pure Grashof convection, i.e. when $Ma = 0$.

The Ohnesorge number Oh is a measure for the relative importance of the viscous forces to the capillary forces. The influence of this number on the temperature, velocity and free boundary is illustrated by figures 5(*a*, *c*, *e*, *g*) for $Oh = 1.0, 0.1, 0.01$ and 0.005 for various values of Gr and $Pr = 0.73$, $Ma = 0$, $Bo = 0$ and by figures 8(*c*, *e*) for $Oh = 0.1$ and 0.01 for two values of Ma and $Gr = 0$, $Pr = 0.73$, $Bo = 0$.

The influence of Oh on the velocity field and on the temperature distribution is very

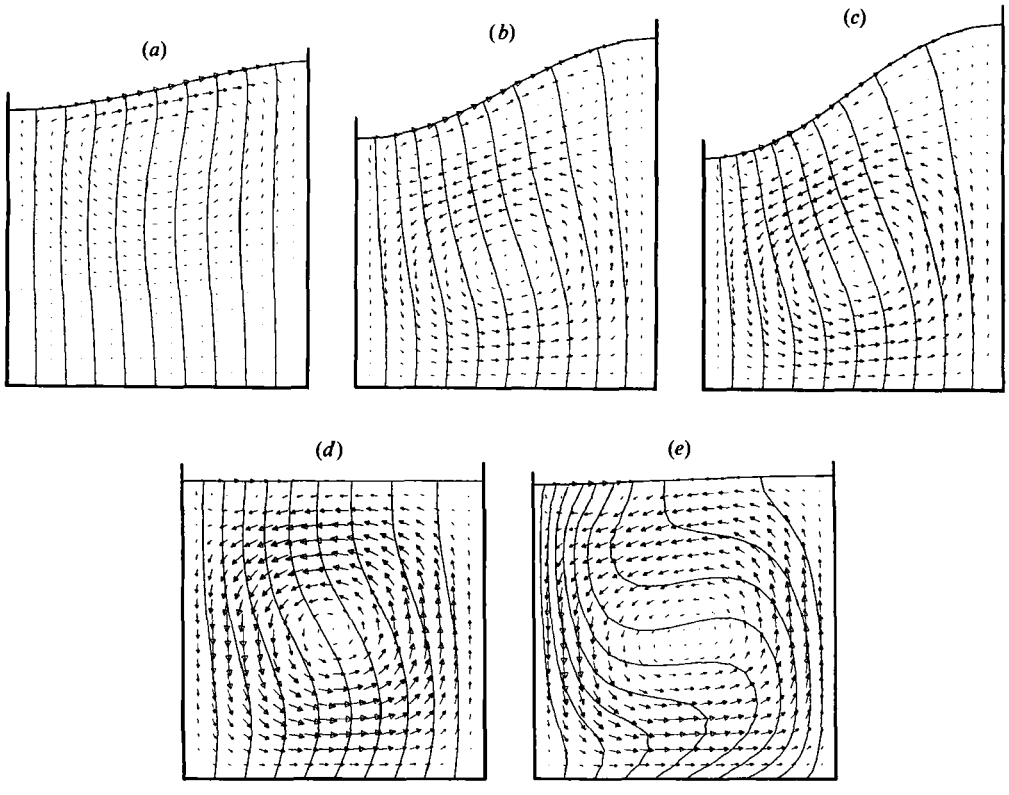

FIGURE 10. The combined effect of Grashof and Marangoni convection: parameters given in table 2.

small. On the other hand, the shape of the free boundary depends strongly on Oh. An increase of the Ohnesorge number has a distorting effect on the free boundary. This phenomenon can be explained from the observation that the Ohnesorge number is proportional to the capillary forces and inversely proportional to the surface-tension coefficient γ_0. When Oh tends to zero, the free boundary approaches the static free boundary.

In the following pictures, we show the combined effect of Grashof and Marangoni convection. Both types of convection induce a clockwise-rotating vortex. In order to study the relative importance of both types of convection, we performed some computations with negative values of the Grashof number, which corresponds, for instance, to a negative volume-expansion coefficient β. Now, the Marangoni convection induces a clockwise vortex, while the vortex due to Grashof convection is in opposite direction. The relative importance of both types of convection is shown in figures 10(a, b, c) where $Pr = 0.73$, $Ma = 50$, $Bo = 0$, $Oh = 0.1$ and $Gr = -200$, -800, -1000. Figures 10(d, e) show the situation for $Pr = 0.73$, $Bo = 0$, $Oh = 0.01$ with $Gr = -1500$, $Ma = 50$ and $Gr = -2 \times 10^4$, $Ma = 300$ respectively.

In figure 10(a) the Marangoni convection dominates the Grashof convection; only one vortex is observed. On increasing the Grashof number (figures 10(b, c)), two counter-rotating vortices appear. The vortex near the free surface is due to Marangoni convection, the vortex in the bulk is a consequence of Grashof convection. A characteristic number indicating the relative importance of Grashof (buoyancy)

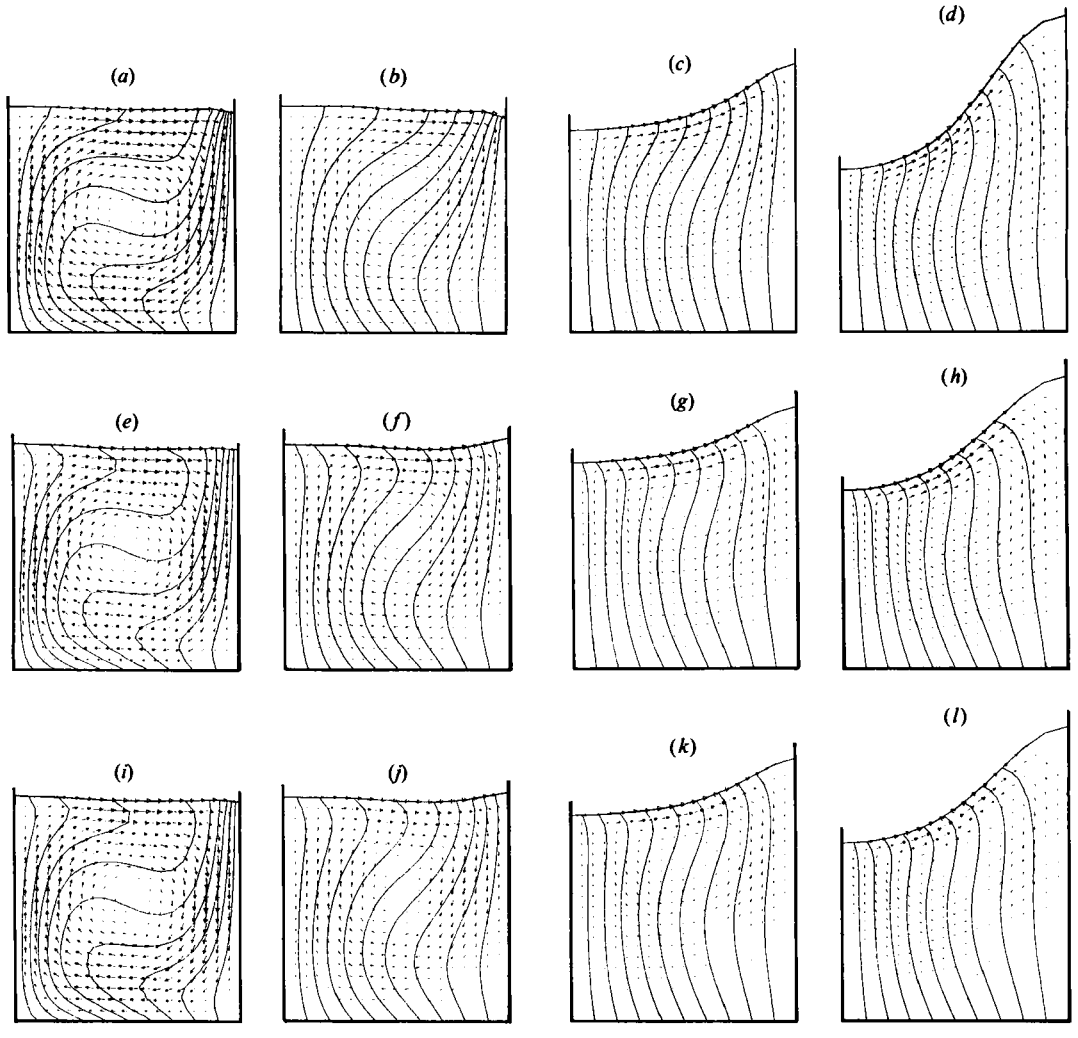

FIGURE 11. The influence of the acceleration due to gravity g on the combined effect of Grashof and Marangoni convection: parameters given in table 2.

convection to Marangoni (thermocapillary) convection is the dynamic Bond number Bd, which for gentle convection is defined by (cf. Ostrach 1977)

$$Bd = \frac{Gr\,Pr}{Ma} = \frac{\beta g \rho_0 L^2}{\alpha \gamma_0}.$$

The values of the dynamic Bond number corresponding to figures 10(*a–c*) are $Bd = 2.9$, 11.7, 14.6 respectively. For the situation of figures 10(*d*, *e*) we have $Bd = 21.9$ and 48.7 respectively. For the two situations of figures 10(*d*, *e*) the Grashof convection is dominant. Nevertheless, we observe a small vortex in the left upper corner of the melt. In this left upper corner the local value of $-\partial T/\partial \tau$ is much larger than the mean value $(T_+ - T_-)/L$ which appears in the definition of the Marangoni number. This means that, locally, the Marangoni convection can be important due to steep gradients in the surface temperature, resulting into a clockwise rotating vortex.

Finally, we show in figures 11 (*a–l*) the influence of the acceleration due to gravity g on the combined effect of Grashof and Marangoni convection for some values of Bi_r and Bi_c. These computations correspond to the situation in which all physical constants are fixed, except for g which is reduced by three times a factor 10 from its terrestrial value. This implies that all characteristic numbers are fixed, except the Grashof and Bond number. We take $Pr = 0.73$, $Ma = 146$, $Oh = 0.1$, $Bi_r = 0$, $Bi_c = 0$ and $Gr = 2 \times 10^4$, $Bo = 10^3$ (figure 11 *a*), $Gr = 2 \times 10^3$, $Bo = 10^2$ (figure 11 *b*), $Gr = 200$, $Bo = 10$ (figure 11 *c*), $Gr = 20$, $Bo = 1.0$ (figure 11 *d*). Corresponding situations are shown in figures 11 (*e–h*) and 11 (*i–l*) for $Bi_r = 2 \times 10^{-4}$, $Bi_c = 0$ and $Bi_r = 0$, $Bi_c = 0.4$ respectively. These computations correspond to the following normalized data for the temperature: $T(x_1 = 0) = 9.0$, $T(x_1 = 1) = 10.0$, $T_0 = 9.5$, $T_{inf} = 8.0$ and $T_{amb} = 8.0$. Isotherms are shown for $T = 9.0$ (0.1) 10.0.

For these situations the dynamic Bond number equals $Bd = 100$, 10, 1.0, 0.1 respectively. We see that for large values of Bd, corresponding to a terrestrial experiment, Grashof convection dominates, while for small values, corresponding to the same experiment in space, Marangoni convection is important. Radiation and cooling flatten the free boundary and influence the temperature field near the free boundary. When the cooling Biot number or the radiation Biot number is increased, a supercooled region (i.e. $T < 9.0$) appears in the right-upper corner of the melt (particularly for large Marangoni numbers, cf. figures 11 *h*, *l*).

In this paper the melt–crystal interface has been considered as constant. For a realistic crystal-growth simulation this free (moving) boundary must be taken into account. The growth rate and the interface shape of the crystal are determined by the heat balance on the interface. For the present situation this means that the isotherm near the crystal reflects the shape of the crystal–melt interface. Figure 11 shows the influence of the gravitation term on the temperature distribution and consequently on the melt–crystal interface. When we consider the isotherm near the crystal, i.e. near $x_1 = 1$, we see that on Earth (cf. figure 11 *a*, *e*, *i*) the growth rate at the bottom is larger than at the top, while in a low-g environment (cf. figures 11 *d*, *h*, *l*) the growth rate at the bottom is smaller than at the top. In a future paper we shall quantify these remarks by numerical experiments.

5. Résumé and Final Remarks

In this paper we have studied a two-dimensional free-boundary problem arising from the steady thermocapillary flow in a viscous fluid whose motion is governed by the Navier–Stokes equations coupled with the heat-conduction equation. The problem is considered in the context of the open-boat technique of crystal growth. The problem is formulated in a non-dimensional form giving rise to the introduction of eight characteristic numbers (*Re*, *Gr*, *Pr*, *Ma*, *Bo*, *Oh*, Bi_r, Bi_c).

For the computation of the free boundary three iterative methods have been studied. The first and second methods are defined as processes which iterate between the free boundary and the flow-field variables (velocity, pressure, temperature), while in the third method the flow-field variables are coupled with the unknown free-boundary nodes. The difference between the first and second method lies in the treatment of the Navier–Stokes equations coupled with the heat equation. For these three methods we have studied the convergence behaviour. We found a linear convergence rate of method one and two, while method three is almost quadratic. Concerning the inner-iterations of methods one and two, we observed that one or two iterations for the solution of the Navier–Stokes equations and the heat equation in

a fixed domain are sufficient. The problem of the Navier–Stokes and heat equation in a fixed domain is discretized by a finite-element method. The incompressibility constraint is verified in a global-penalized way.

Finally a number of numerical experiments are performed, showing the influence of the characteristic numbers Gr, Pr, Ma, Bo, Oh, Bi_r and Bi_c on the flow field variables and on the shape of the free boundary. In this paper a model of an open-boat-type crystal-growth method has been considered. The same computational techniques can be applied to realistic crystal-growth methods. We refer to Chang & Brown (1983), Langlois (1981, 1982) for computations without capillary free boundary and to Chin & Carlson (1983), Derby & Brown (1985) and Witomski (1977) for a finite-element analysis of the thermal capillary model. The Czochralski crystal-growth technique and the floating-zone technique with thermocapillary free boundaries in which the melt–crystal free boundary is also taken into account will form the subject of our future research.

REFERENCES

Allain, G. 1984 Un problème de Navier–Stokes avec surface libre et tension superficielle. In *Proc. Colloque International Problèmes à Frontières Libres, Maubuisson* (to appear).

Barbe, C. 1967 Etude de la tension superficielle des liquides purs et des mélanges. Synthèse des éléments bibliographiques. *Air Liquide Rapport* 57–67 CB/IV.

Batchelor, G. K. 1967 *An Introduction to Fluid Dynamics*. Cambridge University Press.

Beale, J. T. 1984 Large-time regularity of viscous surface waves. *Arch. Rat. Mech. Anal*, **84**, 307–352.

Brice, J. C. 1985 *The Growth of Crystals from the Melt*. North-Holland.

Chang, C. J. & Brown, R. A. 1983 Radial segregation induced by natural convection and melt/solid interface shape in vertical Bridgman growth. *J. Cryst. Growth* **63**, 276–284.

Chin, L. Y. & Carlson, F. M. 1983 Finite element analysis of the control of interface shape in Bridgman crystal growth. *J. Cryst. Growth* **63**, 561–567.

Crouzeix, M. & Raviart, P. A. 1973 Conforming and non-conforming finite element methods for solving the stationary Stokes equations. *RAIRO* **7**, 33–76.

Curruthers, J. R. 1977 Crystal growth in a low gravity environment. *J. Cryst. Growth* **42**, 379–385.

Cuvelier, C. 1982 On the solution of capillary free boundary problems governed by the Navier–Stokes equations. *Rept.* 82–09, Delft University of Technology.

Cuvelier, C. 1985*a* A time dependent free boundary governed by the Navier–Stokes equations, Lecture Notes in Physics, vol. 218, pp. 170–174. Springer.

Cuvelier, C. 1985*b* A capillary free boundary problem governed by the Navier–Stokes equations. *Comput. Meths. Appl. Mech. Engng* **48**, 45–80.

Cuvelier, C., Segal, A. & van Steenhoven, A. A. 1986 *Finite-Element Methods and Navier–Stokes Equations*. Reidel.

Dennis, J. E. & More, J. 1977 Quasi-Newton methods, motivation and theory. *SIAM Rev.* **19**, 46–89.

Derby, J. J. & Brown, R. A. 1983 Finite element analysis of a thermal-capillary model for liquid encapsulated Czochralski growth. *J. Electrochem. Soc.* February, 470–482.

Driessen, J. M. 1984 Effects of non-uniform surface tension in fluid flow: Marangoni effect. Master's thesis, Delft University of Technology.

Engelman, M. S., Strang, G. & Bathe, K. J. 1981 The application of quasi-Newton methods in fluid mechanics. *Intl J. Num. Meth. Engng* **17**, 707–718.

Engelman, M. S. 1984 *Fluid Dynamics Analysis Package FIDAP*. Fluid Dynamics Int.

Greenspan, H. P. 1968 *The Theory of Rotating Fluids*. Cambridge University Press.

Guibert, J. P., Huynh, H. T. & Marce, J. L. 1976 Etude générale de l'influence des liquides contenus dans les satellites *Rep. ESTEC* 2720.

HARDY, S. C. 1985 The surface tension for liquid gallium. *J. Cryst. Growth* **71**, 602–606.

HARTMAN, P. (ed.) 1973 *Crystal Growth: An Introduction*. North-Holland.

HAYNES, J. M. 1979 Fundamental and applied aspects of fluid physics under microgravity. In *Proc. 3rd Symp. on Materials in Space, Grenoble*, ESA SP-142 pp. 275–279.

HURLE, D. T. J. & JAKEMAN, E. 1981 Introduction to the techniques of crystal growth. *PCH: Physico Chemical Hydrodynamics* **2**, 237–244.

JONES, I. P. & THOMSON, C. P. (ed.) 1981 Contribution in numerical solutions for a comparison problem in natural convection in an enclosed cavity. *AERE Harwell*.

KISTLER, S. F. & SCRIVEN, L. E. 1984 Coating flow theory by finite element and asymptotic analysis of the Navier–Stokes system. *Intl J. Numer. Meth. Fluids* **4**, 207–229.

LANDAU, L. D. & LIFCHITZ, E. M. 1963 *Mécanique de Fluides*. Editions MIR Moscou.

LANGLOIS, W. E. 1981 Convection in Czochralski growth melts. *PCH: Physico Chemical Hydrodynamics* **2**, 245–261.

LANGLOIS, W. E. 1982 A parameter sensitivity study for Czochralski bulk flow of silicon. *J. Cryst. Growth* **56**, 15–19.

LIONS, J. L. 1973 Perturbations singulières dans les problèmes aux limites et en contrôle optimal. Lecture Notes in Mathematics, vol. 323. Springer.

MOISEEV, N. N. & RUMYANTSEV, V. V. 1968 *Dynamic Stability of Bodies Containing Fluid*. Springer.

OSTRACH, S. 1976 Convection phenomena of importance for materials processing in space. *COSPAR Symposium on Materials Sciences in Space, Philadelphia*, pp. 2–32.

OSTRACH, S. 1977 Motion induced by capillarity, *PCH: Physico Chemical Hydrodynamics* **2**, 571–589.

OSTRACH, S. 1979 Convection due to surface-tension gradients. *Space Res.* **19**, 563–570.

OSTRACH, S. 1982 Low-gravity fluid flows. *Ann. Rev. Fluid Mech.* **14**, 313–345.

PIMPUTKAR, S. H. & OSTRACH, S. 1981 Convective effects in crystals grown from melt. *J. Cryst. Growth* **55**, 614–646.

PUKHNACHEV, V. V. 1974 Problems with free boundary for the Navier–Stokes equations. Ph.D. thesis, Novosibirsk.

RUSCHAK, K. 1980 A method for incorporating free boundaries with surface tension in finite element fluid-flow simulations. *Intl J. Num. Meth. Engng* **15**, 639–648.

SAITO, H. & SCRIVEN, L. E. 1981 Study of coating flow by the finite element method. *J. Comp. Phys.* **42**, 53–76.

SCHWABE, D. 1981 Marangoni effects in crystal growth melts. *PCH: Physico Chemical Hydrodynamics* **2**, 263–280.

SCHWABE, D. & SCHARMANN, A. 1981 Marangoni convection in open boat and crucible, *J. Cryst. Growth* **52**, 435–449.

SEGAL, A. 1979 A Finite Element Package AFEP. *Rep. Delft University of Technology*.

SOLONNIKOV, V. A. 1979 Solvability of the boundary value problem describing the motion of a viscous incompressible capillary fluid in an open vessel in the two dimensional case. *Izv. Akad. Nauk.* SSR **43**, 203–236.

WITOMSKI, P. 1977 Modélisation et étude numérique d'une expérience de croissance cristalline, Thèse Mathématiques Appliquées Grenoble.